J. Membrane Biol. 179, 13–25 (2001)
DOI: 10.1007/s002320010033

The Journal of
Membrane
Biology



# Effects of Toxins Pi2 and Pi3 on Human T Lymphocyte Kv1.3 Channels: The Role of Glu7 and Lys24

**M. Péter Jr.[1], Z. Varga[1], P. Hajdu[1], R. Gáspár Jr.[1], S. Damjanovich[1], E. Horjales[2], L.D. Possani[2], G. Panyi[1]**

[1]Department of Biophysics and Cell Biology, University Medical School of Debrecen, 4012 Hungary, POB 39
[2]Department of Molecular Recognition and Structural Biology, Institute of Biotechnology, National Autonomous University of Mexico, Avenida Universidad, 2001 Cuernavaca 62210 MEXICO

Received: 17 December 1999/Revised: 3 October 2000

**Abstract.** *Pandinus imperator* scorpion toxins Pi2 and Pi3 differ only by a single amino acid residue (neutral Pro7 in Pi2 *vs.* acidic Glu7 in Pi3). The binding kinetics of these toxins to human Kv1.3 showed that the decreased *on* rate ($k_{ON} = 2.18 \times 10^8$ M$^{-1}$sec$^{-1}$ for Pi2 and $1.28 \times 10^7$ M$^{-1}$sec$^{-1}$ for Pi3) was almost entirely responsible for the increased dissociation constant ($K_d$) of Pi3 ($K_d = 795$ pM) as compared to Pi2 ($K_d = 44$ pM). The ionic strength dependence of the association rates was exactly the same for the two toxins indicating that through-space electrostatic interactions can not account for the different *on* rates. Results were further analyzed on the basis of the three-dimensional structural models of the toxins. A 3D structure of Pi3 was generated from the NMR spectroscopy coordinates of Pi2 by computer modeling. The Pi3 model resulted in a salt bridge between Glu7 and Lys24 in Pi3. Based on this finding our interpretation of the reduced *on* rate of Pi3 is that the intramolecular salt bridge reduces the local positive electrostatic potential around Lys24 resulting in decreased short-range electrostatic interactions during the binding step. To support our finding, we constructed a 3D model of the Ser-10-Asp Charybdotoxin mutant displaying distinctly reduced affinity for *Shaker* channels. The mutant Charybdotoxin structure also displayed a salt bridge between residues Asp10 and Lys27 equivalent to the one between Glu7 and Lys24 in Pi3.

**Key Words:** Human lymphocyte — Kv1.3 — Scorpion toxin binding — *Pandinus imperator* — Charybdotoxin — Three-dimensional structure — Salt bridge

*Correspondence to:* R. Gáspár

## Introduction

The voltage-gated potassium channel, Kv1.3, plays an important role in T-cell physiology because of its involvement in the regulation of the membrane potential of these cells thereby influencing T-cell activation in vitro [4, 18, 21, 34]. $K^+$ channel blocker scorpion toxins (Stox) together with complementary mutagenesis of Kv1.3 proved to be excellent tools in studying structure-function relations and defining binding sites for the blockers on the ion channel [1]. Recently, Stox Kv1.3 channel blocker Margatoxin has been shown to be effective even in suppressing T-cell function in vivo [17]. The above results suggest that Kv1.3 may be an excellent target for modulating immune system functions by specific and potent blockers [3].

During the search for more potent $K^+$ channel inhibitors the whole venom of scorpion *Pandinus imperator* (PiV) has been applied to the voltage-gated potassium channels of nerve fibers and $GH_3$ cells. The effects of the *Pandinus* venom was shown to be different from other known $K^+$ channel Stox in their marked voltage dependence and poor reversibility of the block on these channels [29, 30].

Recently, several new $K^+$ channel blocking peptides named Pi1-Pi7 were purified to homogeneity from the venom of *Pandinus imperator* and their primary structures were determined [14, 26, 27]. Toxins Pi2 and Pi3 are very closely related in their structure, both contain three disulfide bridges and the sequences differ only in one amino acid at position 7 (proline in Pi2 *vs.* glutamic acid in Pi3) in the N-terminal region [14]. Pi2 and Pi3 bear 7 and 6 net positive charges, respectively. The three-dimensional structure of Pi2, under the name of

PTX K-alpha, was determined by NMR spectroscopy [36].

The whole *Pandinus imperator* venom efficiently reduces whole-cell $K^+$ currents in human peripheral blood lymphocytes [32]. Preliminary experiments also showed that purified peptide components Pi2 and Pi3 of the venom powerfully blocked Kv1.3 channels in human peripheral blood lymphocytes with approximate $K_d$ values of 50 pM and 500 pM, respectively [32].

The single amino acid difference between Pi2 and Pi3 and the large difference in their blocking potency for Kv1.3 provide excellent background for studying the structure-function relationship of current block by these toxins. Our experiments were motivated by in-depth analysis of factors influencing toxin binding to *Shaker* and $Ca^{2+}$ activated $K^+$ channels [10, 12, 13, 22, 25, 31, 35]. These include long-range nonspecific electrostatic interactions, short-range electrostatic interactions and close contact steric interactions. The contribution of these interactions to toxin binding requires the analysis of blocking kinetics, the determination of association and dissociation rates and the ionic strength dependence of the rate constants. We applied this approach to determine the difference between the binding of Pi2 and Pi3 to Kv1.3 channels. In addition to patch-clamp experiments we analyzed the results in the view of differences found between the three-dimensional structures of these toxins, as well as between those of relevant charybdotoxin (ChTx) mutants [12].

Throughout this article observations concerning Pi2, one of the most potent toxin inhibitor of Kv1.3, are presented in detail, in comparison with Pi3. Kv1.3 was studied in human peripheral blood lymphocytes where voltage-gated whole-cell currents are dominated by these channels.

## Materials and Methods

### Cells

Heparinized human peripheral venous blood was obtained from healthy volunteers (authors of the paper). Mononuclear cells were separated by Ficoll-Hypaque density gradient centrifugation. Collected cells were washed twice with $Ca^{2+}$- and $Mg^{2+}$-free Hanks' solution containing 25 mM HEPES (pH:7.4). Cells were cultured in a 5% $CO_2$ incubator at 37°C in 24-well culture plates in RPMI-1640 supplemented with 10% FCS (Hyclone, Logan, Utah), 100 u./l penicillin, 100 μg/ml streptomycin and 2 mM L-glutamine at $0.5 \times 10^6$/ml density for 3–4 days. The culture medium also contained 2.5 or 5 μg/ml of phytohemagglutinin A (PHA-P, Sigma-Aldrich Kft, Hungary) to increase $K^+$ channel expression [8, 9].

### Electrophysiology

Whole-cell measurements were carried out using Axopatch-200 and Axopatch-200A amplifiers connected to personal computers using Axon Instruments TL-1-125 and Digidata 1200 computer interfaces, respectively. For data acquisition and analysis the pClamp6 software package (Axon Instruments, Foster City, CA) was used. T lymphocytes were selected for current recording by incubation with mouse anti-human CD2 (Becton-Dickinson, San Jose, CA) followed by selective adhesion to Petri dishes coated with goat anti-mouse IgG antibody (Biosource, Camarilo, CA), as described by Matteson and Deutsch [24]. Dishes were washed gently five times with 1 ml of normal extracellular bath medium (*see below*) for the patch-clamp experiments. Standard whole-cell patch-clamp techniques were used [11, 24, 32, 39]. Series resistance compensation up to 85% was used to minimize voltage errors and achieve good voltage-clamp conditions ($V_{err} < 5$ mV). Pipettes were pulled from GC 150 F-15 borosilicate glass capillaries (Clark Biomedical Instruments, UK) in two stages and fire polished, resulting in electrodes having 2–3 MΩ resistance in the bath. The bath solution was (in mM): 145 NaCl, 5 KCl, 1 $MgCl_2$, 2.5 $CaCl_2$, 5.5 glucose, 10 HEPES (pH 7.35, ionic strength = 190.5 mM). The high ionic strength external solution was (in mM): 77.5 NaCl, 5 KCl, 48.6 $MgCl_2$, 2.5 $CaCl_2$, 5.5 glucose, 10 HEPES (pH 7.35, ionic strength = 265.9 mM). The measured osmolarity of the external solutions was between 302 and 308 mOsm. The pipette solution was (in mM): 140 KF, 11 $K_2$EGTA, 1 $CaCl_2$, 2 $MgCl_2$, and 10 HEPES (pH 7.20, ~295 mOsm).

### Test substances

*Pandinus imperator* venom was obtained from anesthetized animals by electrical stimulation. To separate the peptide toxin components the soluble venom was initially fractionated in a Sephadex G-50 column and the subfractions were further fractionated by high performance liquid chromatography (HPLC), using a C18 reverse-phase column (Vydac, Hysperia, CA), of a Waters 600E HPLC apparatus. The homogeneity of the purified samples was confirmed by step-gradient HPLC and direct Edman degradation using an automatic sequencer [7, 14].

Solutions were supplemented with 0.1 mg/ml bovine serum albumin to suppress nonspecific binding of the toxins to the walls of the tubes and to the Petri dish. Bath perfusion around the measured cell with different test solutions was achieved using a gravity-flow perfusion setup with 8 input lines and PE10 polyethylene tube output tip with flanged aperture to reduce the turbulence of the flow. The solutions were applied in an alternating sequence of control and test solutions, unless stated otherwise. Excess fluid was removed continuously. For the measurement of blocking kinetics of toxins data acquisition was synchronized to fluid exchange using solenoid valves controlled by pClamp6 via digital outputs of Digidata 1200. The reference electrode was connected to the recording chamber with an agar bridge to eliminate junction potential changes during perfusion.

### Data Analysis

Prior to analysis whole-cell current traces were corrected for ohmic leak and digitally filtered (3 point boxcar smoothing). Nonlinear least squares fits were done using the Marquardt-Levenberg algorithm. Fits were evaluated visually, as well as by the residuals and the sum of squared differences between the measured and calculated data points.

Statistical comparisons were made using Student's *t*-test, and when appropriate, paired *t* test at $P = 0.05$. For all experiments, the standard error of the mean (SEM) is reported.

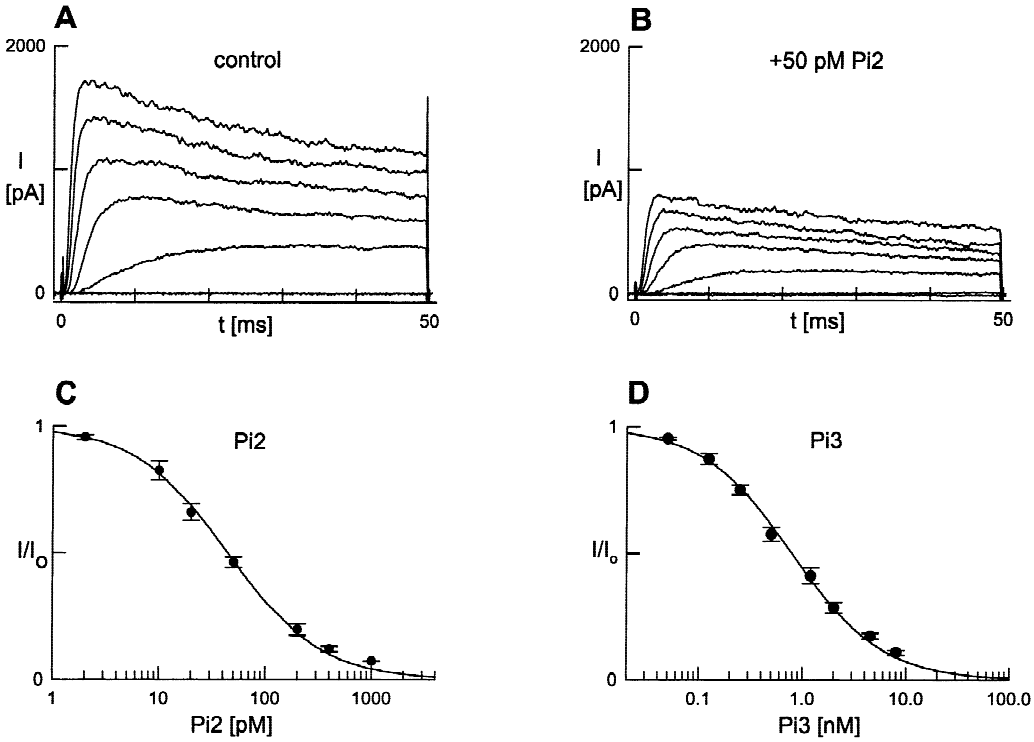


**Fig. 1.** Effects of Pi2 and Pi3 on whole-cell $K^+$ currents in human T lymphocytes. (*Panel A*) Lymphocyte perfused with control extracellular solution. Voltage steps lasting for 50 msec were applied every 50 sec from a holding potential of −80 mV in 10 mV increments from −70 to +50 mV. Selected traces are displayed only for image clarity (−70, −50, −30, −10, 10, 30, 50 mV). (*Panel B*) Whole-cell $K^+$ currents of the same cell in the presence of 50 pM Pi2 using the same pulse protocol as for *panel A*. Sampling rate was 20 kHz, lowpass filtering was applied at 5 kHz. Current traces were smoothed using the 3-point boxcar method. (*Panels C and D*) Dose response of $K^+$ current block by Pi2 and Pi3, respectively. The fraction of unblocked current was calculated as $I/I_o$, where $I_o$ is the peak $K^+$ current measured in the control solution and $I$ is the peak current during bath perfusion with the test solution containing the toxin. The solid line is the binding curve fitted to the data points based on a 1:1 drug:channel stoichiometry: $I/I_o = K_d/(K_d + [Tx])$, where $[Tx]$ indicates the toxin concentration and $K_d$ is the dissociation constant. The best fit resulted in a dissociation constant of 44 and 795 pM for Pi2 and Pi3, respectively. The test potential was +50 mV, the holding potential was −120 mV. Error bars indicate SEM ($n = 3$).

### Modeling of 3D-Structures of Pi3 and the Ser-10-Asp ChTx Mutant

The 3D-structure of Pi2 toxin from the scorpion *Pandinus imperator* was obtained as a multiple NMR structure from the Brookhaven Protein Data Bank, entry 2PTA [36]. The conformation with best geometry (first reported in the entry) was used to model Pi3. A direct mutation command was used in the program "O" [15] and applied to position 7 to change the side chain from Pro to Glu, to obtain a first-step structure in the modeling procedure. This step was natural since the Ramachandran angles of the Pro7 residue in Pi2 structure are compatible with a Glu in that position (phi = −77, psi = −29). Next, ROTAMER search command was applied, to find the rotamer with the best interactions. Thus the second most frequent rotamer for the Glu was selected. We also changed the Lys24 rotamer so this residue could build the salt bridge with Glu7. As no repulsive interactions were found in this conformation and no main-chain tensions were generated with this point-mutation we decided to use this model without further optimization. Moreover, the salt bridge geometry generated (*see* Results) is both natural and compatible with experimental observations in this work. The 3D-structure of wild-type ChTx was obtained from the Brookhaven Protein Data Bank, entry 2CRD [2]. The Ser-10-Asp mutant of ChTx was built in the same way as for Pi3 and the resulting rotamers were also the same.

## Results

### Pi2 and Pi3 block Kv1.3 Channels with High Affinity

Figure 1*A* shows whole-cell current traces recorded from a human T lymphocyte. Currents were evoked from −80 mV holding potential at test potentials ranging from −70 to +50 mV. Under the experimental conditions used in this study, i.e., low internal $Ca^{++}$ (*see* Materials and Methods) the current traces correspond to voltage-gated potassium current flowing through Kv1.3 channels of human T lymphocytes. Figure 1*B* shows that 50 pM Pi2 reduced the above demonstrated whole-cell $K^+$ currents effectively at all membrane potentials tested (*see below*).

Dose dependence of equilibrium $K^+$ channel block by Pi2 and Pi3 was determined by measuring the peak whole-cell $K^+$ current at +50mV in the bath solution ($I_o$) then changing the perfusion to bath solutions containing the toxins at different concentrations. To verify that equilibrium block was reached, short (50 msec duration)

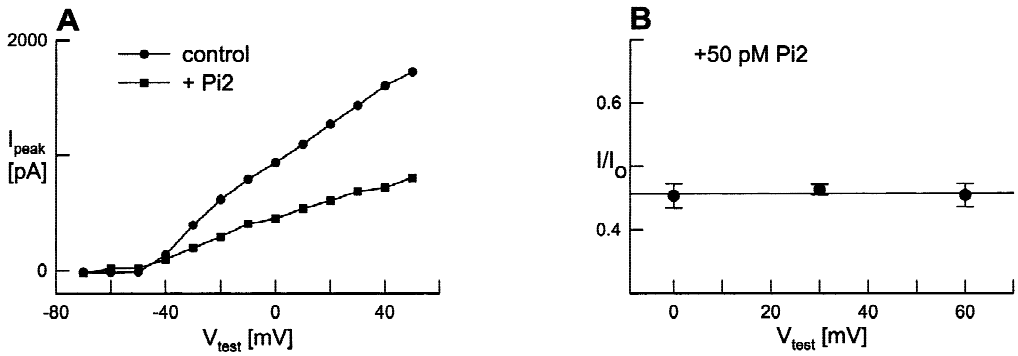


**Fig. 2.** Block of Kv1.3 by Pi2 is voltage independent. (*Panel A*) Peak currents derived from the measurement represented in Fig. 1*A* and *B* and plotted as a function of applied test potential. *Control:* (●); 50 pM Pi2: (■). (*Panel B*) Remaining fractions of the whole-cell $K^+$ current in a human T lymphocyte at different test potentials during perfusion with 50 pM Pi2. Remaining fractions were calculated as $I/I_o$ where $I_o$ is the peak of the control current and $I$ is the peak in the presence of 50 pM Pi2. Cells were depolarized from −120 to 0, +30 and +60 mV for 50 msec. Data were fitted with a straight line with the equation: $I/I_o = SL \times TP + INT$, where $SL$ is the slope of the line, $TP$ is the applied test potential and $INT$ is the $y$ intercept. The fit yielded $1.7 \times 10^{-5}$ 1/mV for slope.

depolarizing pulses to +50 mV were applied every 50 sec. The peak current in the presence of the toxin ($I$) was calculated by averaging 3–4 peaks at equilibrium block. From $I_o$ and $I$ the remaining fraction ($R = I/I_o$) of the current was calculated and plotted as a function of toxin concentration in Fig. 1*C* and *D* for Pi2 and Pi3, respectively. The resulting dose response curve could be fitted by equation $R = K_d/(K_d + [Tx])$ describing a model where one toxin molecule binds to one channel protein. In the above formula $R$ indicates the remaining fraction of the whole-cell current, $[Tx]$ is the extracellular toxin concentration and $K_d$ is the dissociation constant characterizing the drug-channel interaction. The excellent fit obtained supports a mechanism in which one toxin molecule binds to one channel protein and plugs the pore of the channel similarly to ChTx [13]. As a result of the fitting procedure $K_d = 44$ pM and $K_d = 795$ pM were obtained for Pi2 and Pi3, respectively. Both toxins bind to the voltage-gated Kv1.3 channels of human T lymphocytes with high affinity.

## Block by Pi2 and Pi3 Shows No Voltage Dependence

Pappone et al. reported previously a voltage-dependent action of the whole soluble venom on delayed rectifier $K^+$ channels of myelinated frog nerve fiber [29]. In our previous paper we showed that no voltage dependence of block exists for the full *Pandinus imperator* venom on human T lymphocyte $K^+$ channels [32]. Pi2 bears a net 7 positive charge and has a lysine in position 24 equivalent to the lysine in position 27 of ChTx, which is critical for interaction with *Shaker* potassium channels. However, other charged and uncharged amino acids in several positions influence their binding affinity. To further examine the reasons for the above-mentioned difference in the voltage dependence of the $K^+$ channel block by the *Pandinus imperator* venom we tested the effect of toxins Pi2 and Pi3 purified from the whole venom on the voltage dependence of the block. We determined the remaining fraction of whole-cell current in the presence of 50 pM Pi2 at various membrane potentials. Current-voltage relations on Kv1.3 show that the percentage of block by Pi2 is independent of the applied test potential (Fig. 2*A* and 2*B*). Similar results proved the voltage independence of the Pi3 block (*data not shown*). The voltage independence of the block in both cases implies that the binding site of the highly charged toxin component on Kv1.3 is not deeply immersed into the transmembrane electric field. Alternatively, the rate of obtaining a new equilibrium at different depolarized membrane potentials is not fast enough to show the voltage dependence of the block measured from the peak current (*see* Discussion).

## Association and Dissociation of Pi2 and Pi3 are Very Fast

$K^+$ channel block by Pi2 and Pi3 is reversible, because after washing toxin-treated human T lymphocytes with drug free extracellular solution the whole-cell $K^+$ current returns to its original amplitude (Fig. 3). The very low dissociation constant of Pi2 and the fact that its blocking effect was fully reversible by washing in less than 15 min, suggested that the *on* and *off* rates of the toxin are very high. Therefore, we examined the association and dissociation rates of Pi2 to the channel protein by determining the wash-in and wash-out kinetics of the drug on

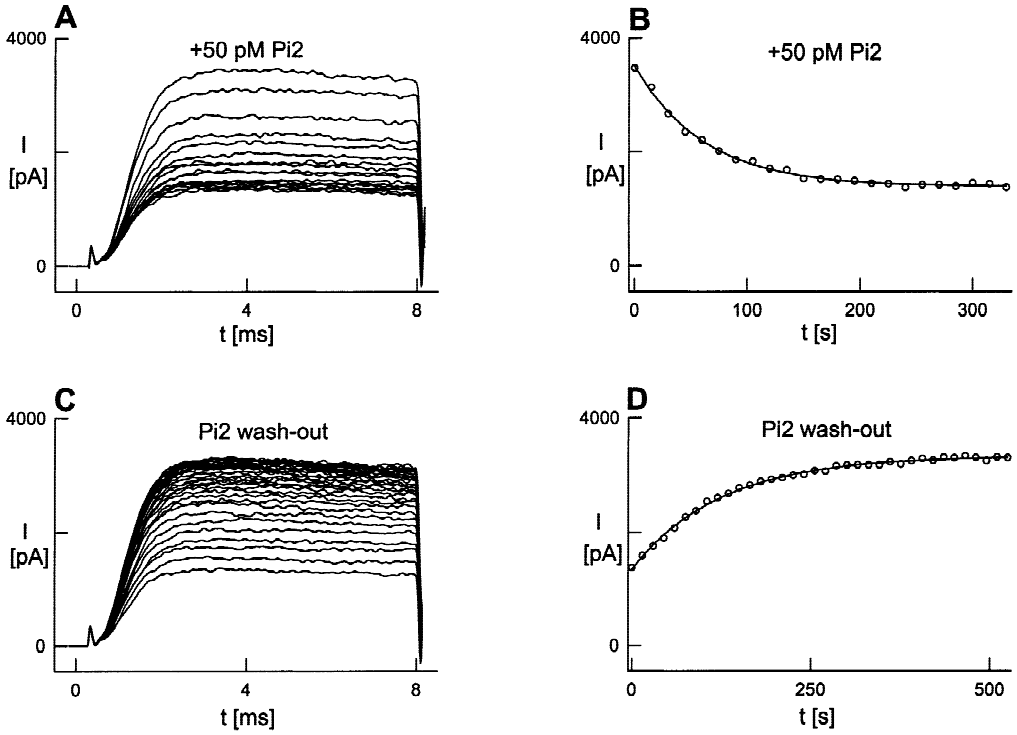


**Fig. 3.** Wash-in and wash-out kinetics of Pi2 characterizing the interaction of the toxin with Kv1.3 channels of human T lymphocytes. Cells were held at a holding potential of −120 mV and depolarized for 8 msec to +50 mV at every 15 sec. The bath was perfused with control extracellular solution until the current amplitude stabilized. (*Panel A*) The perfusion was switched to solution containing 50 pM Pi2 by the use of electromagnetic valves driven by the computer at the end of the first episode shown. The perfusion with toxin containing solution was continuous until equilibrium block was reached. (*Panel B*) Peak currents were plotted as the function of time and fitted to a single exponential decay (*see* the text for details). (*Panel C*) After the equilibrium block had already been reached the perfusion was switched back to control solution by the software driven valves. (*Panel D*) The peak whole-cell $K^+$ currents were plotted against the time elapsed from switching back to the control solution and were fitted to a single exponential rise.

the Kv1.3 channels of human T lymphocytes in the whole-cell configuration (Fig. 3). To achieve a good time resolution we used depolarizing pulses lasting for 8 msec only, and applied every 15 sec (Fig. 3*A* and *C*). This pulsing rate did not induce cumulative inactivation since identical peak amplitudes were obtained after wash-out compared to those measured at the beginning of the wash-in process. The gravity-driven flow of extracellular solution was switched on and off by electromagnetic valves controlled by the data acquisition apparatus.

The measurement of the time course of current block by the toxin was started after the peak amplitude stabilized when entering whole-cell. Whole-cell $K^+$ currents recorded after switching to an extracellular solution containing 50 pM Pi2 (Fig. 3*A*) and peak values were plotted in Fig. 3*B* as a function of time and fitted to a single exponential function: $A(t) = B \times \exp(-t/T_{ON}) + C$, where $A(t)$ indicates the amplitude of the measured current at time $t$, $C$ is the peak current at equilibrium block and $B = A(t = 0) - C$. The time constant ($T_{ON}$) describing the wash-in kinetics of Pi2 yields 58 ± 7 sec ($n = 7$). After reaching equilibrium block of the whole-cell current the perfusion was switched back to the drug-free control solution, while the voltage-clamp protocol recording the whole-cell current was running continuously. The results are displayed in Fig. 3*C*. Peak currents recorded during the wash-out procedure were plotted the same way as above (Fig. 3*D*) and were also fitted to a single exponential function: $A(t) = B \times (1 - \exp(-t/T_{OFF})) + C$, where $B = A(t = \infty) - C$, $A(t)$ and $C$ were defined above. The resulting time constant ($T_{OFF}$) was 158 ± 21 sec ($n = 7$) in this case.

$K^+$ channel block by Pi3 was also found to be reversible (*data not shown*). We determined the time constants of block and unblock by 500 pM Pi3 using the same method as above. For Pi3 the values of $T_{ON}$ and $T_{OFF}$ were 53 ± 3 sec ($n = 8$) and 80 ± 6 sec ($n = 7$), respectively. From the measured time constants and assuming a simple bimolecular reaction between the toxin and the channel, $k_{ON}$, $k_{OFF}$ and $K_d$ can be expressed as follows:

**Table 1.** Blocking parameters of Pi2 and Pi3 in normal and high ionic strength solutions*

| | Solution | $k_{ON}$ ($M^{-1}sec^{-1}$) | $k_{OFF}$ ($sec^{-1}$) | $K_d$ |
|---|---|---|---|---|
| Pi2 | NR** | $2.18 \times 10^8$ | $6.33 \times 10^{-3}$ | 29 pM |
| | HIS*** | $6.90 \times 10^6$ | $17.7 \times 10^{-3}$ | 2558 pM |
| Pi3 | NR** | $1.28 \times 10^7$ | $12.5 \times 10^{-3}$ | 0.97 nM |
| | HIS*** | $3.98 \times 10^5$ | $18.0 \times 10^{-3}$ | 45.2 nM |

* Second-order association and first-order dissociation rates were determined from averaged $T_{ON}$ and $T_{OFF}$ values obtained from 4–7 independent wash-in-wash-out experiments. $K_d$ was calculated as the ratio of kinetic constants $k_{OFF}/k_{ON}$. **Normal Ringer solution. ***High ionic strength solution.

$$k_{ON} = \frac{1 - T_{ON} \times k_{OFF}}{T_{ON} \times [Tx]}, \quad k_{OFF} = \frac{1}{T_{OFF}}, \quad K_d = \frac{k_{OFF}}{k_{ON}}.$$

The calculated values of $k_{ON}$, $k_{OFF}$ and $K_d$ are displayed in Table 1.

### Association Rate of Pi2 and Pi3 is Sensitive to the Ionic Strength of the Solution

To study the influence of through-solution electrostatic interaction between the cationic toxin and the anionic mouth of the ion channel on the kinetics of ion channel blockade the effect of increasing ionic strength of the extracellular solution was assayed. In high ionic strength solution (HIS), the concentration of divalent magensium ions was raised in the recording solution to 48.6 mM while the osmolarity of the solution was kept constant for undisturbed patch-clamping of human lymphocytes (*see* Materials and Methods). The isosmotic substitution resulted in a 1.4-fold increase in the ionic strength. We determined the dissociation constants, the *on* and the *off* rates of Pi2 and Pi3 in HIS and compared them to the ones measured in normal Ringer (NR) solution (*see* Table 1). In the high ionic strength solution *on* rates decreased 32-fold for both toxins, when *off* rates increased 2.8- and 1.4-fold altogether causing 88- and 46-fold increased dissociation constants for Pi2 and Pi3, respectively.

### Pi2 Alters the Kinetics of Recovery from Inactivation of Kv1.3 Channels

In our previous paper [32] we reported that current block by the whole soluble Pi venom is associated with a significant enhancement of the rate of recovery from inactivation of Kv1.3. In this paper we extended this study to the purified Pi2 and Pi3 peptides of the venom. In the presence of Pi2 the recovery from inactivation of human lymphocyte Kv1.3 channels became faster (Fig. 4). During the experiments we applied 1 sec long depolarizing pulse pairs with various interepisode intervals ranging from 1 to 60 sec (Fig. 4*A*). The 1 sec long test pulse was

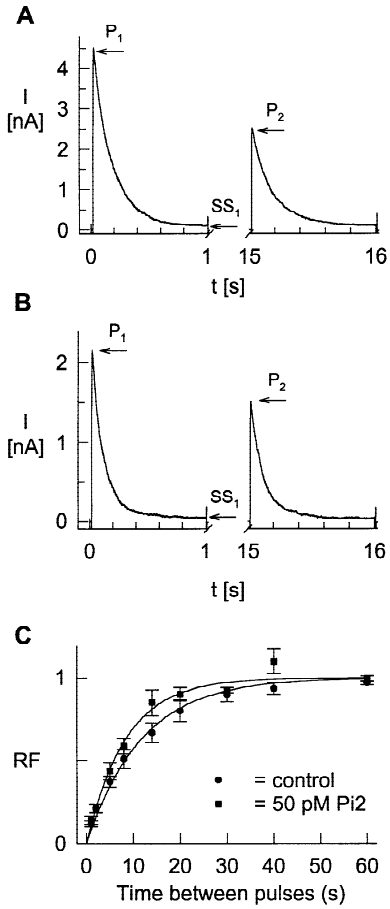


**Fig. 4.** The effect of 50 pM Pi2 on recovery from inactivation of Kv1.3 channels in human T lymphocytes. (*Panel A*) Representative whole cell currents evoked by a pulse pair (1 sec to +50 mV) separated by 14 sec interpulse interval at −120 mV holding potential in control solution. $P_1$ and $P_2$ are peak currents observed during the first and second pulses, respectively, and $SS_1$ is the steady-state current at the end of the first pulse. The recovered fraction (*RF*) of the channels was calculated using the following formula: $RF = (P_2\text{-}SS_1)/(P_1\text{-}SS_1)$. The calculated RF was 0.55 in this experiment. (*Panel B*) Recovery from inactivation in the presence of Pi2 is faster. The same cell as in *Panel A* was perfused with 50 pM Pi2. All other experimental conditions were the same. 50 pM Pi2 reduced the peak current to 48% of control. The calculated *RF* was 0.70 indicating that 70% of the inactivated channels recovered from inactivation within 14 sec. The value of RF is higher in the presence of Pi2 than in the absence. (*Panel C*) Comparison of the kinetics of recovery from inactivation in the presence and absence of Pi2. Depolarizing pulse pairs (1 sec to +50 mV) separated by various inter-pulse intervals ranging from 1 to 60 sec were applied. The time between pulse pair sequences was 80 sec at −120 mV holding potential to allow full recovery of the channels. The recovered fraction (*RF*) of the channels was calculated as above. Mean ± SEM ($n = 3$) of *RF* is plotted on the figure for control solutions (●) and obtained during bath perfusion with 50 pM Pi2 (■) as a function of interpulse interval. The continuous lines show the best fit to a single exponential function (*see* text).

enough for reaching steady-state amplitude for the whole-cell current. Time between pulse pairs was 80 sec at a holding potential of −120 mV to allow full recovery of the channels. We calculated the fraction of channels (*RF*) recovered from the inactivated state during the varying interpulse intervals using the formula $RF = (P_2 - SS_1)/(P_1 - SS_1)$, where $P_1$ and $P_2$ are peak currents detected during the first and the second pulses in the pair, respectively and $SS_1$ is the steady-state amplitude of the current during the first pulse. Figure 4*B* shows the two-pulse protocol applied to the same cell in the presence of 50 pM Pi2. The RF increased from 0.55 in control solution (Fig. 4*A*) to 0.70 (Fig. 4*B*) indicating that channels recover faster from inactivation in the presence of Pi2. We determined the recovery time constant by plotting the recovered fractions as the function of interpulse interval and fitting a single exponential function: $RF(t) = 1 - \exp(-t/T)$ to the data points. Recovery from inactivation was significantly accelerated in the presence of 50 pM Pi2, because the time constant characterizing it decreased from 15.42 ± 1.87 sec (control) to 10.42 ± 1.04 sec ($P < 0.0028$, $n = 6$).

One amino acid difference between Pi2 and Pi3 caused an 18-fold difference in their affinity for Kv1.3 as determined from the equilibrium block of the channels. We were interested to know if the ability of Pi2 and Pi3 to speed up recovery from inactivation of Kv1.3 was different. Any such existing difference could be immediately attributed to the mutated amino acid in position 7 (Glu for Pro), between the two toxins.

In the previous section we have shown that recovery from inactivation was a single exponential process. Therefore, in order to characterize the effect of toxins on the recovery kinetics, it was sufficient to compare *RF* values obtained at fixed time intervals under control conditions and after the application of Pi2 or Pi3. We have chosen 7 sec interpulse intervals and applied close to half blocking concentrations of Pi2 (44 pM) and Pi3 (500 pM). We used the 7 sec long inter-episode time because by this time the recovered fraction of the current was close to 0.5. We calculated the recovered fractions of the channels in the control extracellular solution and in solutions containing Pi2 and Pi3. The recovered fraction of the $K^+$ current during the 7 sec long inter-episode time was 0.53 ± 0.03 in the absence and 0.56 ± 0.03 in the presence of 500 pM Pi3 ($P < 0.099$, $n = 6$). Using the same protocol the recovery from inactivation was accelerated by Pi2 resulting in a recovered current fraction 0.53 ± 0.05 compared to the control value of 0.45 ± 0.02. The latter difference proved to be significant (paired *t*-test, $P < 0.009$, $n = 5$). The observed difference in the ability of Pi2 and Pi3 to speed up the recovery from inactivation of Kv1.3 can only be associated to the seventh amino acid in the toxins, which is the only different amino acid in these peptides.

### Three-Dimensional Model of Pi3

Based on the parameters obtained from NMR spectroscopy data of Pi2 [36], a model of the three-dimensional structure of Pi3 was generated, as described in Materials and Methods. This independently generated model was fully compatible with the recently published 3D NMR structure of Pi3 [16].

Pi3 is a natural mutant (Pro-7-Glu) of Pi2, in which the substituted proline for glutamic acid in position 7 does not modify the folding pattern of the molecule, on the contrary, the distances and angle torsion constraints are quite compatible with the formation of a salt bridge with Lys24, as shown in Fig. 5. Lys24 of Pi2 and Pi3 is at the equivalent structural position of Lys27 in ChTx [12], (Table 2) and Lys28 in noxiustoxin [23]. Both lysines were shown to be essential for binding to the K-channels studied [33]. Figure 5*A* represents Pi2, whereas Fig. 5*B* is the model of Pi3. The colored amino acids are some of those found to be essential for toxin-channel interaction, plus residue 7, which is the mutated amino acid. In magenta is Lys24, in white, from left to right are Phe33, Lys31, Met26 and Asn27. In blue is Pro7 for Pi2 and Glu7 for Pi3, making the salt bridge with Lys24.

### Three-Dimensional Model of the Ser-10-Asp ChTx Mutant

Earlier work performed by the group of Miller [12] showed that a mutant of ChTx containing an aspartic acid in position 10, substituting for serine, was capable of recognizing the channel with 1,500-fold less affinity, compared to native ChTx. When we aligned the amino acid sequences of these peptides in search for the best similarity, we observed that Ser10 of ChTx corresponds to position 7 in Pi2, where the glutamic acid substitutes for proline in Pi3 (Table 2). Thus, the three-dimensional models of wild-type ChTx (Fig. 5*C*) and its mutant containing aspartic acid (Fig. 5*D*) were constructed on the basis of literature data and compared to our results. The Asp10 has a spatial geometry compatible with a salt-bridge formation with Lys27 in the mutant ChTx. These results are consistent with the highly conserved structural folding of the segments where these mutations occur in Pi2 and ChTx. Position 10 in ChTx and position 7 in Pi2, are the first residues of the alpha-helical domains of the toxins, whereas residue 27 in ChTx (24 in Pi2) is a central residue in one of the conserved beta-strands of these peptides. Consequently, the relative positions of the mutated residues are compatible with the formation of salt bridges in both Pi3 and Ser-10-Asp ChTx, which could explain an important decrement of affinity (increase of $K_d$) for the respective channel.

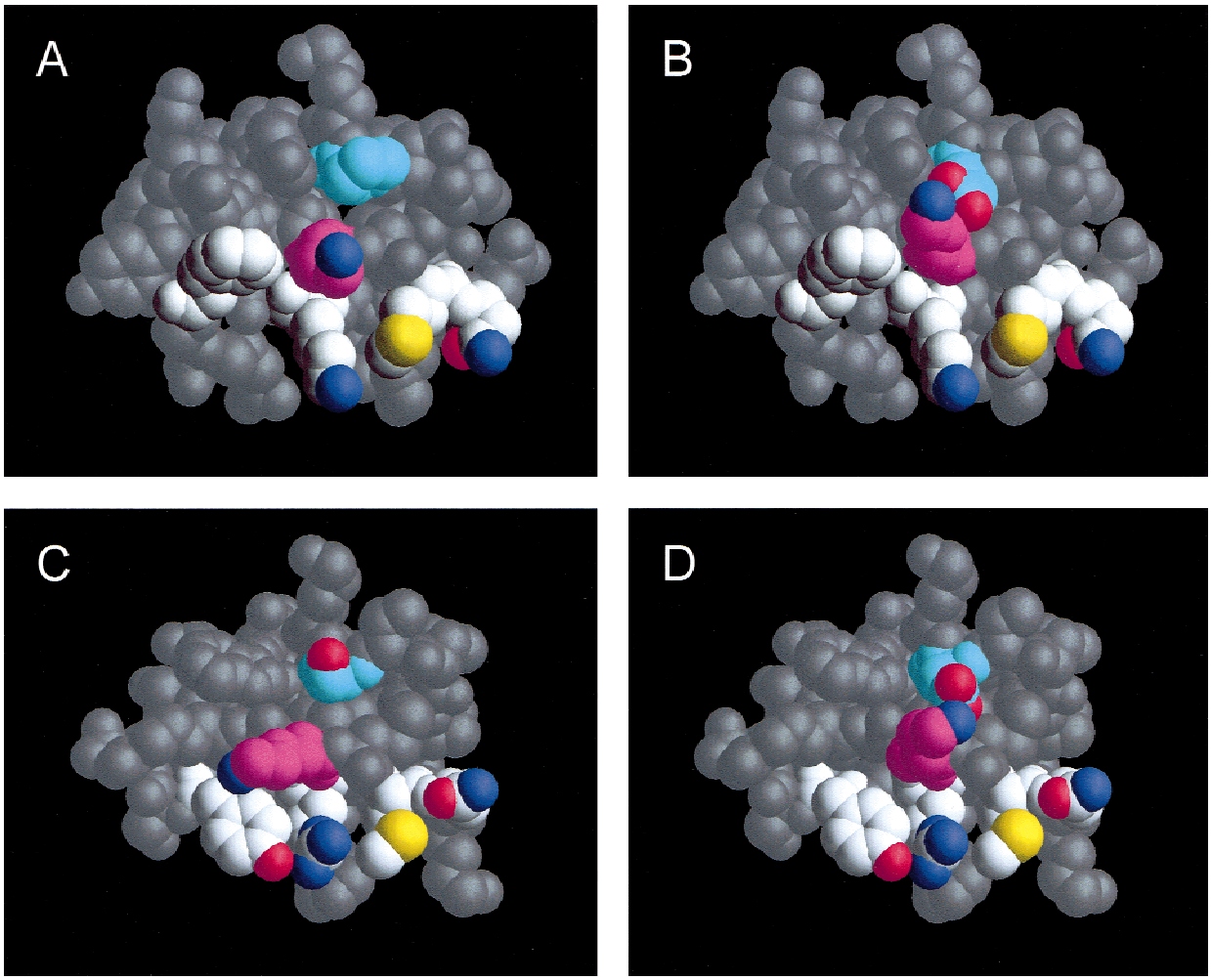


**Fig. 5.** Three-dimensional models of Pi2, Pi3, wild-type ChTx and Ser-10-Asp mutant of ChTx. (*Panel A*) A view of the Pi2 structure observed from the Lys24 residue (with carbon atom in magenta). Some amino acids essential for channel binding (from left to right: Phe33, Lys31, Met26 and Asn27) are represented with carbon atoms in white. Pro7, the only point mutation differentiating Pi2 and Pi3 is represented in cyan. Other atom types in these residues are colored, as follows: oxygen in red, nitrogen in blue and sulfur in yellow. The remaining structure is shown in gray. (*Panel B*) Pi3 toxin model viewed in the same orientation as *panel A*; color codes are also the same as above. A movement of the Lys24 (in magenta) is observed, thus, this amino acid is in adequate geometry to build a salt bridge with Glu7 (in cyan), still being in its second most frequent rotamer. (*Panel C*) A view of the wild-type ChTx structure, observed from the Lys27 residue. Color codes are as in *Panel A* for the corresponding residues in the sequence alignment. (Ser10 in cyan, Lys27 in magenta). The spatial similarity of the conformations of Ser10 and Pro7 of Pi2 can be observed. (*Panel D*) Structure of the Ser-10-Asp mutant of ChTx viewed in the same orientation as in *Panel C;* color codes are also the same. The salt bridge Lys27-Asp10 presents a geometry very similar to that of the Pi3 model, thus explaining the observed decrease in affinity for the channel.

## Discussion

In the present work we describe the effect of peptide toxin components Pi2 and Pi3 of the *Pandinus imperator* scorpion venom on the Kv1.3 type voltage-gated $K^+$ channel of human T lymphocytes. Earlier, we published results on the effect of the whole venom on Kv1.3 channels and preliminary data on the dissociation constants characterizing three peptide components of the venom [32]. We further investigated Pi2 as it had the highest affinity among the toxins indicated by a very low dissociation constant and Pi3 because of its very similar structure to Pi2.

In general, channel blockers can be pore blockers or gating modifiers. Pore blockers bind to the channel in 1:1 stoichiometry and plug the pore of the channel impeding the flow of the ionic current. Our data suggest that both Pi2 and Pi3 belong to the pore blocker family. This fact is supported by the following properties of the equilibrium block and the blocking kinetics of the compounds. The dose-response curve can be fitted well to a function describing a one channel–one blocker model

**Table 2.** Primary structure of Pi2, Pi3, ChTx and Ser-10-Asp mutant ChTx*

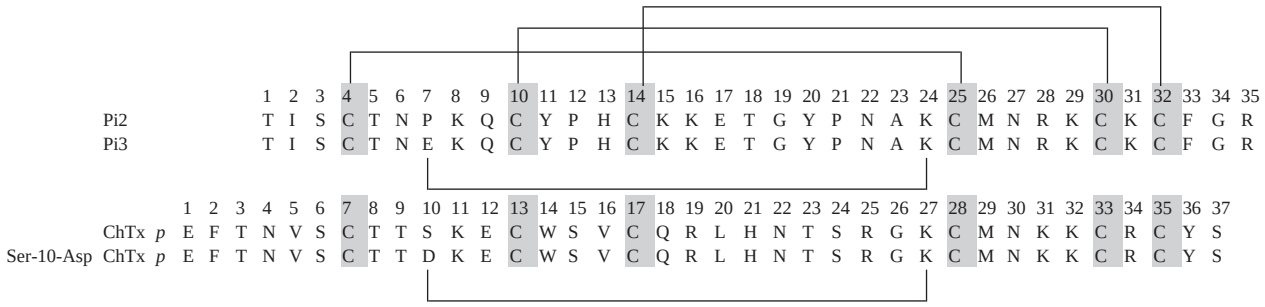


* Structures were aligned in search for best similarity in the amino acid sequences of these peptides. Position of the salt bridge (indicated by connecting lines under the text) formed between the residues Asp10 and Lys27 in the Ser-10-Asp mutant of ChTx corresponds exactly to the one formed between Glu7 and Lys24 in Pi3. Disulfide bridges are indicated by the connecting lines above the sequence.

(Fig. 2*A*). We also investigated the wash-in and wash-out kinetics of the toxins and found that both of them follow a single exponential time course. This behavior is characteristic of first order (dissociation) and pseudo first order (association) bimolecular reactions.

We determined the dissociation constant of Pi2 from both the equilibrium block and the *on* and *off* rates of the toxin molecules binding to the channel protein. The first approach resulted in a $K_d = 44$ pM for Pi2, whereas the calculated $K_d$ from the *on* and *off* rates was 29 pM. These data are comparable and support the 1:1 stoichiometry of Pi2 binding to Kv1.3 channels. We also determined the dissociation constant of Pi3 using both methods. The $K_d$ of Pi3 was 795 pM according to the equilibrium method and 970 pM calculated from the *on* and *off* rates, again leading to a reasonable agreement of the results.

If the binding site of a channel blocker is deeply immersed into the electric field of the cell membrane, and the blocker is a charged particle like Pi2, the block may show voltage dependence. The whole soluble venom of scorpion *Pandinus imperator* showed highly voltage-dependent block on voltage-gated $K^+$ channels of nerve fibers [29]. Our experiments, however, did not show voltage dependence of the block by Pi2 and Pi3 on voltage-gated $K^+$ channels of human T lymphocytes, although both toxins were positively charged pore blockers of the channels. This is not surprising if we consider the time course of channel activation and the *on* and *off* rates of the block. The time needed to reach the peak of the current depends on the amplitude of the test pulse but it is always in the msec range. *On* and *off* rates determined experimentally were in the order of seconds. The block of Kv1.3 channels by Pi2 and Pi3 may be voltage dependent although this fact is not seen in our results, where we determined the remaining fractions of the $K^+$ current from the peak amplitudes measured at different test potentials. It can be assumed that the peak of the current is reached much faster during a test pulse than the time necessary for the development of a new equilibrium of block at the currently applied test potential. Indeed, Goldstein and Miller studied the voltage dependence of current block by several low affinity mutants of ChTx (*e.g.*, Y36A) having high *off* rate. The voltage dependence of block in those cases could be determined from equilibration of block during a single depolarizing pulse [13].

The only difference between Pi2 and Pi3 is the presence of a negatively charged amino acid in Pi3 (Glu7), resulting in an 18-fold increase of the $K_d$ as determined from the equilibrium block of the channels. The analysis of blocking kinetics of Kv1.3 channels isolated that the 17-fold decrease of Pi3 *on* rate was primarily responsible for the increase of $K_d$, since the change of the *off* rate was negligible (only 2-fold increase over Pi2). The minimal increase of Pi3 *off* rate indicates that the Pro to Glu change did not alter the steric interactions between the channel and the toxin [12]. This means that steric hindrance for binding to Kv1.3 was not generated by the amino acid substitution.

At the same time, the Pro-7-Glu mutation in Pi3 results in a decrease in the net positive charge of the toxin, which might influence the long-range electrostatic interaction between the channel and the toxin. Several authors discussed previously the importance of through-space electrostatics in toxin binding by introducing charge neutralization or charge reversal mutations either in the channel vestibule or in the toxin [10, 12, 22, 25, 31]. Simple electrostatics predicts that charge alterations should be manifested in the association rate of the toxin. Indeed, mutations decreasing the net charge of ChTx [12, 31] and Iberiotoxin [25] decreased the toxin *on* rates. Similarly, substituting acidic residues for neutral or basic ones near the toxin binding site (position 422 in *Shaker*) also decreased the association rate of ChTx [12] and toxin Lq2 [10]. Our experiments showed that the association (*on*) rate of Pi3 (bearing net 6 positive charges)

was 17-times smaller than that of Pi2 (bearing net 7 positive charges), while the *off* rates were comparable (Table 1). So far our results are compatible with the predictions from through-space electrostatics. This model, however, also predicts that (i) increasing the ionic strength of the recording solution should decrease the association rate of the toxins, and (ii) the ionic strength dependence of the association rate should be more pronounced for Pi2 (+7 charges) as compared to Pi3 (+6 charges). Our results showed that the *on* rate of both Pi2 and Pi3 was reduced when the ionic strength was raised (Table 1). At the same time, the association rate of Pi2 and Pi3 was equally sensitive to the ionic strength of the medium, the 1.4-fold increase in the ionic strength resulted in a 32-fold decrease in the association rate of both toxins. These results pointed out that through-space electrostatics is an important factor for toxin binding but glutamic acid residue at position 7 in Pi3 does not contribute significantly to the overall long-range electrostatic interaction, similarly to ChTx mutations studied by Park and Miller [31]. Thus, through-space electrostatics can not account for the decreased association rate of Pi3.

So what can be the explanation for the reduced *on* rate of Pi3? To answer this question the model of the three-dimensional structure of Pi3 was generated based on the parameters obtained from NMR spectroscopy data of Pi2. This model showed that glutamic acid in position 7 (Pi3) is likely to form a salt bridge with Lys24. Lys24 of Pi2 and Pi3 is at the equivalent structural position of Lys27 in ChTx that is essential for toxin binding to $K^+$ channels. To examine the effect of the salt bridge between Glu7 and Lys24 we applied the analysis of non-diffusion-limited bimolecular toxin-channel interactions used by Escobar et al. [10] and Mullmann et al. [25]. This approach considers a two-step reaction for toxin binding (Scheme 1). The first step includes diffusion of the toxin (*Tx*) up to and away from the encounter complex (*EC*). This step accounts for the local electrical potential and ionic strength dependence of the association rate (*see above*, Table 1, Eqs. 6 and 7 in Escobar et al. [10]). The *EC* represents an infinite number of possible contact orientations formed between the toxin (*Tx*) and the channel (*C*) from which the bound state of the toxin (*B*) is formed in the second step. In nondiffusion controlled reactions this second step is the rate-limiting and might include the rearrangement of amino acid side chains, formation of hydrogen bonds and squeezing water molecules and cations out of the vestibule to form the tightly bound (nonconducting) toxin:channel complex.

Scheme 1:

$$Tx + C \rightleftarrows EC \rightleftarrows B$$

The second (binding) step would allow specific short-range electrostatic interactions between specific basic residues on the toxin and cations in the vestibule. Accordingly, Mullmann et al. [25] argued that neutralization of Lys27 and Arg34 reduces the ability of IbTx mutants to repel cations from the vestibule, which would account for the 10- to 20-fold slower association rate of Lys-27-Gln, Lys-27-Asn and Arg-34-Asn mutants. Our results are similar to these data both qualitatively and quantitatively (Table 1). Thus, our interpretation of the reduced *on* rate of Pi3 is that the intramolecular salt bridge formed between Glu7 and Lys24 reduces local positive electrostatic potential around Lys24 resulting in decreased short-range electrostatic interactions during the binding step. This might lead to a decreased association rate by a similar mechanism to the one described above for IbTx mutants.

The ϵ-amino group of Lys-27 in ChTx protrudes slightly into the $K^+$ conduction pore, where it interacts with conducting ions [13]. Does the salt bridge between Lys24 and Glu7 break up during the binding step to allow Lys24 to interact freely with the ion channel? The overall free energy change calculated for the binding of Pi2 and Pi3, based on the $K_d$, $k_{ON}$ and $k_{OFF}$ values obtained is 58.5 kJ/mol for Pi2 and 51.4 kJ/mol for Pi3. The difference is in the order of 7 kJ/mol, a value that is not enough to break a salt bridge (approx. 15 kJ/mol). This means that besides the salt bridge, other interactions are implicated in the overall free energy change observed, either through the interaction of the carboxylate of the glutamic acid with some other residues in the channel, or even with the formation of hydrogen bonds or van der Waals interactions between residues of the toxin and the channel. The overall free energy change due to these interactions may easily compensate for the free energy change during the breaking of the salt bridge. It is certainly true that the overall free energy change for Pi2 is higher than Pi3 and thus it goes into the right direction of the expected results, assuming our proposition of salt bridge formation in Pi3 and its breaking during the interaction of the toxin with the channel.

The influence of salt bridge formation on binding of Pi3 to Kv1.3 is further substantiated by a comparison of the present problem to the binding of a ChTx mutant to a similar ion channel, the *Shaker* $K^+$ channel [12]. A considerable difference between the affinity of the wild-type ChTx and its Ser-10-Asp mutant has been observed to the *Shaker* $K^+$ channel. According to the sequence alignment in Table 2 positions 7 and 24 in Pi2 correspond to positions 10 and 27 in ChTx, respectively. Mutation of Ser to an acidic residue (Asp) in position 10 of ChTx resulted in a 1,500-fold increase in the equilibrium dissociation constant for the *Shaker* channel [12]. At the same time the 3D molecular modeling performed by us

pointed out the existence of a salt bridge between the Asp10 and Lys27 positions in the Ser-10-Asp mutant ChTx that is similar to the salt bridge between corresponding positions in Pi3. Thus, a similar mechanism, as discussed above for Pi3, can account for the observed high $K_d$ of the Ser-10-Asp mutant ChTx [12].

Our salt bridge hypothesis is strongly supported by a recent paper in which the three-dimensional structure of Pi3 was determined by NMR spectroscopy and compared to that of Pi2 [16]. They determined that the overall folding pattern of Pi3 was very similar to Pi2. In addition, a salt bridge between Glu7 and Lys24 of Pi3 was described. Based exclusively on NMR spectroscopy data the authors attributed the reduced affinity of Pi3 to the intramolecular salt bridge between Glu7 and Lys24 [16]. Although both our results and the results of Klenk et al. support the idea that the salt bridge between Glu7 and Lys24 explains the lowered affinity of Pi3 for the Kv1.3 channel, in the absence of toxin docking models, we can not exclude the possibility that the two toxins bind with slightly different geometry to the Kv1.3 turret and pore.

Since our three-dimensional models of Pi2, Pi3 and ChTx showed the possibility of salt bridge formation between acidic residues of position around 7–10 with the lysine in position 24–27, we looked into the literature for other homologues. Recently, a paper by Tytgat et al. [37] proposed a generalized nomenclature for K-scorpion toxin subfamilies, and listed 49 complete amino acid sequences (now 50, *see* ref. [5]). Examination of all these peptides suggests that none of them (except Pi3) would qualify for such salt bridge formation. The only other two toxins with acidic residues around residue 10 are two novel toxins, PBTX1 and PBTX2 purified from scorpions of the genus *Parabuthus* of South Africa [38]. These toxins belong to subfamily 11 and were reported to have a low affinity for $K^+$-channels, however they contain a valine in the position 26 (equivalent to Lys27 of ChTx), which would make impossible a salt bridge formation in this spatial location.

Dauplais et al. [6] reported recently that structurally unrelated highly specific potassium channel inhibitor toxins possess an essential dyad consisting of a critical Lys and a neighboring aromatic residue separated by ~7 Å. According to the sequence alignment in Table 2, Lys24 and Phe33 qualify for that dyad in Pi2 and Pi3. Our molecular models in Fig. 5 show the close position of the corresponding residues on the contact surface of both Pi2 and Pi3. The calculated distance between the $C_\alpha$ carbon atoms of Lys24 and Phe33 is 7.9 Å which is in a good agreement with the distance (6.6 ± 1 Å) between $C_\alpha$ of the critical Lys and the center of the benzene rings of the neighboring tyrosines in toxins BgK and ChTx [6]. Thus, Pi2 and Pi3 contain the conserved critical residues for potassium channel blocking.

Recently, we found that the whole soluble venom of the scorpion *Pandinus imperator* accelerates the recovery from inactivation of Kv1.3 channels [32]. We investigated the same effect for purified Pi2, which is the most effective peptide component of the *Pandinus imperator* venom on Kv1.3 channels. We found that Pi2 accelerates the recovery from inactivation of Kv1.3 channels. This means that the toxin remains bound to the inactivated channel and destabilizes this conformation. The ability of Pi2 to speed up the recovery from inactivation of Kv1.3 channels is remarkable.

The kinetics of dissociation of Pi2 and Pi3 from Kv1.3 is relatively fast, the characteristic time constants are ~180 and 58 sec, respectively. The fast dissociation provides that during the recovery process substantial number of on-off reactions take place to account for the enhanced recovery from inactivation measured in the presence of Pi2. We compared the ability of Pi2 and Pi3 to speed up the recovery from inactivation of human lymphocyte voltage-gated $K^+$ channel, Kv1.3. Recovery from inactivation is enhanced by Pi2, but not by Pi3. This means that the single amino acid difference between the two toxins affects the ability of enhancing the recovery rate of Kv1.3. We do not know yet the nature of molecular interactions responsible for this difference. Due to the complexity of C-type inactivation and recovery several mechanisms might be involved [28]. For example toxins bound to the channel pore might alter diversely the extracellular $K^+$ modulatory site of recovery from inactivation [19, 20].

In conclusion, we described the effects of two potent and closely related peptide toxins on the Kv1.3 channels in human T lymphocytes and gave an explanation for the observed differences in their channel blocking ability and binding kinetics on the basis of the differences in their 3D structures and by comparing them to structurally related ChTx mutants. Due to its remarkably low dissociation constant of 44 pM, Pi2 may provide a good model for developing a nonpeptide drug that could be used to achieve an immunosuppressive effect by specifically blocking human lymphocyte voltage-gated $K^+$ channels.

The authors thank Dr. Vilmos Gáspár for the valuable discussions on the energetics of binding. This work was supported by grants ETT T05/102/2000, OTKA T029947 and FKFP 327/2000 to R.G., OTKA T23873 and T30411 to S.D., FKFP 622/2000, OTKA F035251 and US-Hungarian Joint Fund JFNo.542 to G.P. and grant (75197-527107) from the Howard Hughes Medical Institute to L.D.P. The technical assistance of M.Sc. Timoteo Olamendi-Portugal is greatly acknowledged.

## References

1. Aiyar, J., Withka, J.M., Rizzi, J.P., Singleton, D.H., Andrews, G.C., Lin, W., Boyd, J., Hanson, D.C., Simon, M., Dethlefs, B., Lee, C., Hall, J.E., Gutman, G.A., Chandy, K.G. 1995. Topology

of the pore-region of a $K^+$ channel revealed by the NMR- derived structures of scorpion toxins. *Neuron* **15:**1169–1181

2. Bontems, F., Gilquin, B., Roumestand, C., Menez, A., Toma, F. 1992. Analysis of side-chain organization on a refined model of charybdotoxin: structural and functional implications. *Biochemistry* **31:**7756-7764
3. Cahalan, M.D., Chandy, K.G. 1997. Ion channels in the immune system as targets for immunosuppression. *Curr. Opin. Biotechnol.* **8:**749–756
4. Chandy, K.G., Decoursey, T.E., Cahalan, M.D., McLaughlin, C., Gupta, S. 1984. Voltage-gated potassium channels are required for human T lymphocyte activation. *J. Exp. Med.* **160:**369–385
5. D'Suze, G., Zamudio, F., Gomez Lagunas, F., Possani, L.D. 1999. A novel $K^+$ channel blocking toxin from Tityus descrepans scorpion venom. *FEBS Lett.* **456:**146–148
6. Dauplais, M., Lecoq, A., Song, J., Cotton, J., Jamin, N., Gilquin, B., Roumestand, C., Vita, C., de Medeiros, C.L.C., Rowan, E.G., Harvey, A.L., Menez, A. 1997. On the Convergent Evolution of Animal Toxins. *J. Biol. Chem.* **272:**4302–4309
7. Delepierre, M., Prochnicka Chalufour, A., Possani, L.D. 1997. A novel potassium channel blocking toxin from the scorpion *Pandinus imperator:* A 1H NMR analysis using a nano-NMR probe. *Biochemistry* **36:**2649–2658
8. Deutsch, C., Krause, D., Lee, S.C. 1986. Voltage-gated potassium conductance in human T lymphocytes stimulated with phorbol ester. *J. Physiol.* **372:**405–423
9. Deutsch, C., Price, M., Lee, S., King, V.F., Garcia, M.L. 1991. Characterization of high affinity binding sites for charybdotoxin in human T lymphocytes. Evidence for association with the voltage-gated $K^+$ channel. *J. Biol. Chem.* **266:**3668–3674
10. Escobar, L., Root, M.J., MacKinnon, R. 1993. Influence of protein surface charge on the bimolecular kinetics of a potassium channel peptide inhibitor. *Biochemistry* **32:**6982–6987
11. Gáspár, R., Panyi, G., Krasznai, Z., Ypey, D.L., Vereb, Gy., Pieri, C., Damjanovich, S. 1994. Effects of bretylium tosilate on voltage-gated potassium channels in human T lymphocytes. *Mol. Pharmacol.* **46:**762–766
12. Goldstein, S.A., Pheasant, D.J., Miller, C. 1994. The charybdotoxin receptor of a *Shaker* $K^+$ channel: peptide and channel residues mediating molecular recognition. *Neuron* **12:**1377–1388
13. Goldstein, S.A., Miller, C. 1993. Mechanism of charybdotoxin block of a voltage-gated $K^+$ channel. *Biophys. J.* **65:**1613–1619
14. Gomez-Lagunas, F., Olamendi-Portugal, T., Zamudio, F.Z., Possani, L.D. 1996. Two novel toxins from the venom of the scorpion *Pandinus imperator* show that the N-terminal amino acid sequence is important for their affinities towards *Shaker* B $K^+$ channels. *J. Membrane Biol.* **152:**49–56
15. Jones, T.A., Zou, J.Y., Cowan, S.W., Kjeldgaard. 1991. Improved methods for binding protein models in electron density maps and the location of errors in these models. *Acta Crystallogr. A.* **47:**110–119
16. Klenk, K.C., Tenenholz, T.C., Matteson, D.R., Rogowski, R.S., Blaustein, M.P., Weber, D.J. 2000. Structural and functional differences of two toxins from the scorpion *Pandinus imperator*. *Proteins* **38:**441–449
17. Koo, G.C., Blake, J.T., Talento, A., Nguyen, M., Lin, S., Sirotina, A., Shah, K., Mulvany, K., Hora, D., Jr., Cunningham, P., Wunderler, D.L., McManus, O.B., Slaughter, R., Bugianesi, R., Felix, J., Garcia, M., Williamson, J., Kaczorowski, G., Sigal, N.H., Springer, M.S., Feeney, W. 1997. Blockade of the voltage-gated potassium channel Kv1.3 inhibits immune responses in vivo. *J. Immunol.* **158:**5120–5128
18. Leonard, R., Garcia, M.L., Slaughter, R.S., and Reuben, J.P. 1992. Selective blockers of voltage-gated $K^+$ channels depolarize human T lymphocytes: Mechanism of the antiproliferative effect of charybdotoxin. *Proc. Natl. Acad. Sci. U.S.A.* **89:**10094–10098
19. Levy, D.I., Deutsch, C. 1996*a*. A voltage dependent role for $K^+$ in recovery from C-type inactivation. *Biophys. J.* **71:**3157–3166
20. Levy, D.I., Deutsch, C. 1996*b*. Recovery from C-type inactivation is modulated by extracellular potassium. *Biophys. J.* **70:**798–805
21. Lin, C.S., Boltz, R.C., Blake, J.T., Nguyen, M., Talento, A., Fischer, P.A., Springer, M.S., Sigal, N.H., Slaughter, R.S., Garcia, M.L., Kaczorowski, G.J., Koo, G.C. 1993. Voltage-gated potassium channels regulate calcium-dependent pathways involved in human T lymphocye activation. *J. Exp. Med.* **177:**637–645
22. MacKinnon, R., Miller, C. 1989. Mutant potassium channels with altered binding of charybdotoxin, a pore-blocking peptide. *Science* **245:**1382–1385
23. Martinez, F., Munoz Garay, C., Gurrola, G., Darszon, A., Possani, L.D., and Becerril, B. 1998. Site-directed mutants of noxiustoxin reveal specific interactions with potassium channels. *FEBS Lett.* **429:**381–384
24. Matteson, D.R., Deutsch, C. 1984. $K^+$ channels in T lymphocytes: a patch clamp study using monoclonal antibody adhesion. *Nature* **307:**468–471
25. Mullmann, T.J., Munujos, P., Garcia, M.L., Giangiacomo, K.M. 1999. Electrostatic mutations in Iberiotoxin as a unique tool for probing the electrostatic structure of the Maxi-K channel outer vestibule. *Biochemistry* **38:**2395–2402
26. Olamendi-Portugal, T., Gomez-Lagunas, F., Gurrola, G.B., Possani, L.D. 1996. A novel structural class of $K^+$-channel blocking toxin from the scorpion *Pandinus imperator*. *Biochem. J.* **315:**977–981
27. Olamendi Portugal, T., Gomez Lagunas, F., Gurrola, G.B., Possani, L.D. 1998. Two similar peptides from the venom of the scorpion *Pandinus imperator*, one highly effective blocker and the other inactive on $K^+$ channels. *Toxicon* **36:**759–770
28. Panyi, G., Sheng, Z.-F., Tu, L.-W., Deutsch, C. 1995. C-type inactivation of a voltage-gated $K^+$ channel occurs by a cooperative mechanism. *Biophys. J.* **69:**896–904
29. Pappone, P.A., Cahalan, M.D. 1987. *Pandinus imperator* scorpion venom blocks voltage-gated potassium channels in nerve fibers. *J. Neurosci.* **7:**3300–3305
30. Pappone, P.A., Lucero, M.T. 1988. *Pandinus imperator* scorpion venom blocks voltage-gated potassium channels in GH3 cells. *J. Gen. Physiol.* **91:**817–833
31. Park, C.S., Miller, C. 1992. Mapping function to structure in a channel-blocking peptide: electrostatic mutants of charybdotoxin. *Biochemistry* **31:**7749–7755
32. Péter, M., Varga, Z., Panyi, G., Bene, L., Damjanovich, S., Pieri, C., Possani, L.D., and Gáspár, R. 1998. *Pandinus imperator* scorpion venom blocks voltage-gated $K^+$ channels in human lymphocytes. *Biochem. Biophys. Res. Commun.* **242:**621–625
33. Possani, L.D., Selisko, B., Gurrola Briones, G. 1999. Structure and function of scorpion toxins affecting $K^+$ channels. *Perspectives in drug discovery and design* **15/16:**15–40
34. Price, M., Lee, S.C., Deutsch, C. 1989. Charybdotoxin inhibits proliferation and interleukin 2 production in human peripheral blood lymphocytes. *Proc. Natl. Acad. Sci. USA* **86:**10171–10175
35. Stocker, M., Miller, C. 1994. Electrostatic distance geometry in a $K^+$ channel vestibule. *Proc. Natl. Acad. Sci. USA* **91:**9509–9513

36. Tenenholz, T.C., Rogowski, R.S., Collins, J.H., Blaustein, M.P., Weber, D.J. 1997. Solution structure for Pandinus toxin K-alpha (PiTX-K alpha), a selective blocker of A-type potassium channels. *Biochemistry* **36:**2763–2771
37. Tytgat, J., Chandy, K.G., Garcia, M.L., Gutman, G.A., Martin-Eauclaire, M.F., van der Walt, J.J., Possani, L.D. 1999. A unified nomenclature for short-chain peptides isolated from scorpion venoms; alpha-KTx molecular subfamilies. *Trends in Pharmacological Science* **20:**444–447
38. Tytgat, J., Debont, T., Rostoll, K., Vandenberghe, I., Desmet, F., Verdonck, F., Daenens, P., Van Beeumen, J., van der Walt, J.J. 1998. Novel scorpion $K^+$ channel toxins isolated from venoms of species belonging to the *Parabuthus* genus. *Biophys. J.* **74:***A*229 (*Abst.*)
39. Varga, Z., Bene, L., Pieri, C., Damjanovich, S., Gáspár, R.J. 1996. The effect of juglone on the membrane potential and whole-cell $K^+$ currents of human lymphocytes. *Biochem. Biophys. Res. Commun.* **218:**828–832